Ecological Modelling 294 (2014) 94–104

Contents lists available at ScienceDirect

Ecological Modelling

journal homepage: www.elsevier.com/locate/ecolmodel

Optimization of water uptake and photosynthetic parameters in an ecosystem model using tower flux data

Liming He [a,*], Jing M. Chen [a,**], Jane Liu [a], Gang Mo [a], Stéphane Bélair [b], Ting Zheng [a], Rong Wang [a], Bin Chen [a], Holly Croft [a], M.Altaf Arain [c], Alan G. Barr [d]

[a] Department of Geography and Program in Planning, University of Toronto, 100 St. George St., Room 5047, Toronto, ON M5S 3G3, Canada
[b] Meteorological Research Division, Environment Canada, Dorval, QC H9P 1J3, Canada
[c] School of Geography and Earth Sciences and McMaster Center for Climate Change, McMaster University, Hamilton, ON, L8S4K1, Canada
[d] Climate Research Division, Environment Canada, Saskatoon, SK, Canada

ARTICLE INFO

Article history:
Received 22 May 2014
Received in revised form 19 September 2014
Accepted 25 September 2014
Available online 9 October 2014

Keywords:
Ecosystem model
Parameter optimization
EnKF
Temporal scale
V_{cmax}
Soil water uptake

ABSTRACT

The soil water stress factor (f_w) and the maximum photosynthetic carboxylation rate at 25 °C (V_{cmax}) are two of the most important parameters for estimating evapotranspiration and carbon uptake of vegetation. Ecologically these two parameters have different temporal variations and thus their optimization in ecosystem models poses a challenge. To minimize the temporal scale effect, we propose a three-stage approach to optimize these two parameters using an ensemble Kalman filter (EnKF), based on observations of latent heat (LE) and gross primary productivity (GPP) fluxes at three flux tower sites in 2009. First, the EnKF is applied daily to obtain precursor estimates of V_{cmax} and f_w. Then, V_{cmax} is optimized at different time scales, assuming f_w is unchanged from the first step. The best temporal period is then determined by analyzing the coefficient of determination (R^2) of GPP and LE between simulation and observation. Finally, the daily f_w value is optimized for rain-free days corresponding to the V_{cmax} curve from the best temporal period. We found that the variations of optimized f_w are largely explained by soil water content in the summer. In the spring, the optimized f_w shows a smooth increase following the rise of soil temperature, indicating that f_w may respond to the development of fine roots, which is related to the amount of accumulated heat in the soil. The optimized V_{cmax} generally follows a pattern of a rapid increase at the leaf expansion stage in the spring, small variation in summer, and an abrupt decrease at foliage senescence. With eddy covariance fluxes data, data assimilation with a EnKF can retrieve the seasonal variations of water uptake and photosynthetic parameters in an ecosystem model, and such gives clues on how to model forest responses to water stress.

1. Introduction

Terrestrial ecosystem models have been widely used to simulate carbon, water and energy fluxes and climate-ecosystem interactions (Dietze et al., 2011; Stoy et al., 2013). In these models, some vegetation and soil parameters are determined without consideration of their seasonal variations (Kattge et al., 2009). Data assimilation (DA) provides an effective way to optimize these parameters at different time scales (Kattge et al., 2009; Liu et al., 2012; Pauwels et al., 2007; Pipunic et al., 2008; Rayner, 2010; Wolf et al., 2006). Characterization of the seasonal variations of key ecosystem parameters is important in improving the performance of ecosystem models as the outcomes of the models generally respond to these parameters non-linearly (Wang et al., 2001).

The soil water stress factor (f_w) used in the stomatal conductance formulation and the maximum photosynthetic carboxylation rate at 25 °C (V_{cmax}) are identified as two of the most important parameters related to the estimation of evapotranspiration and carbon uptake of vegetation (Ju et al., 2010; Mo et al., 2008; Wolf et al., 2006; Zhou et al., 2013 Zhu et al., 2009). The existing literature uses different seasonal patterns of these two parameters with different response to soil water depletion (Zhou et al., 2013):

(1) the soil water stress on photosynthesis has been implemented arguably either by adjusting V_{cmax} and/or J_{max} (maximum

* Corresponding author. Tel.: +1 416 978 5070.
** Corresponding author. Tel.: +1 416 978 7085; fax: +1 416 946 3886.
E-mail addresses: liming.he@gmail.com, liming.he@utoronto.ca (L. He), chenj@geog.utoronto.ca (J.M. Chen).

http://dx.doi.org/10.1016/j.ecolmodel.2014.09.019
0304-3800/

electron transport rate) (Cai and Dang, 2002; Dai et al., 2004; Grassi et al., 2005; Wang et al., 2007; Wang et al., 2001; Xu and Baldocchi, 2003), or modifying the slope of the Ball–Woodrow–Berry (BWB) equation (Arain et al., 2006; Bonan, 1995; Heroult et al., 2013; Ju et al., 2006; Wang and Leuning, 1998), or both (Ju et al., 2010; Keenan et al., 2009, 2010b; Reichstein et al., 2003);

(2) a soil water stress factor f_w has been used to modify the original BWB equation (Ball et al., 1987) to include the important influence of soil water on stomatal conductance, but the mathematical form describing the influence differs in different studies. The form has been treated using linear (Arain et al., 2002; Bonan, 1995; Wang and Leuning, 1998; Wang et al., 2001), exponential, or power functions (Bonan, 1995; Ju et al., 2006). Various values of the slope of the BWB equation are reported (Heroult et al., 2013; Ju et al., 2010; Medlyn et al., 2011; Mo et al., 2008; Wolf et al., 2006). f_w was found to vary rapidly in response to soil water dynamics in the root zone (Vicente-Serrano et al., 2013).

(3) the temporal variation of V_{cmax} is often ignored or simply parameterized. In addition to its strong dependence on temperature (Medlyn et al., 2002), V_{cmax} has been found to be linearly (Houborg et al., 2013; Kattge et al., 2009) or non-linearly (Arain et al., 2006) related to leaf Rubisco-N (nitrogen). As the leaf N accumulates and depletes slowly through daily uptake and consumption in photosynthesis, we would not expect that the amount of Rubisco changes quickly on day-to-day basis (Yasumura et al., 2006). This intrinsic V_{cmax} can be inverted from the leaf photosynthesis measurement using Farquhar model (Farquhar et al., 1980) in optimal condition. Earlier studies suggested that DA of vegetation parameters at daily time steps leads to fast changing V_{cmax} values that are unrealistic (Ju et al., 2010; Mo et al., 2008). This is because that the original Farquhar's model has no clear mechanism to describe how photosynthesis will change under stress conditions, such as the deactivation of Rubisco by extreme temperatures and soil water stress (Jensen, 2000), the breakdown of chlorophyll and the importance of mesophyll conductance (Keenan et al., 2010a). So a V_{cmax} inverted from the Farquhar's model under stress condition will have projected information from the missing model structures and apparently have larger temporal variations (Grassi and Magnani, 2005; Reichstein et al., 2003), and often is called "observed V_{cmax}" or "apparent V_{cmax}" (Zhou et al., 2013). The variations of apparent V_{cmax} are modulated by slow variation of leaf N and variations of unexplained model structures (Keenan et al., 2010a).

In short, the temporal variations of these two parameters are in need of further investigation. In this study, we attempt to develop a new optimization scheme that can capture the temporal variation patterns of f_w and V_{cmax} based on measured water and carbon fluxes at three eddy covariance tower sites. Our objectives are: (1) to investigate how N-determined V_{cmax} varies seasonally in forest ecosystems; (2) to find the optimal time window, ranging from 1 day to 15 days, for determining V_{cmax} temporal variability; (3) to examine relationship between f_w and soil volumetric water content (VWC) in the root zone; and (4) to investigate if f_w is directly related to soil temperature when soil water is not the limiting factor in the early and late growth season.

2. Method and data

The boreal ecosystem productivity simulator (BEPS) ecosystem model (Chen et al., 1999, 2007, 2012) is used in this study. A full conceptual diagram of the model is described in Ju et al. (2006). It is a process-based ecosystem model that includes carbon, water, and energy budgets and soil thermal transfer modules. The gross primary productivity (GPP) is modeled by scaling Farquhar's leaf-level biochemical model (Farquhar et al., 1980) up to canopy-level using the "two-leaf" approach (Chen et al., 1999; Norman, 1982). The bulk stomatal conductance of the sunlit and shaded leaves for water vapor and CO_2 is calculated using a modified BWB equation (Ball et al., 1987). The evaporation of intercepted water from the canopy and the ground surface is calculated using the Penman–Monteith equation (Monteith, 1965), and canopy transpiration from sunlit and shaded leaves is computed following Wang and Leuning (1998). The N-weighted V_{cmax} for sunlit and shaded leaves are obtained by taking account of the vertical profile of leaf N content and canopy structure (Chen et al., 2012). The BEPS model is described in detail below.

2.1. Photosynthesis

The canopy-level photosynthesis (A_{canopy}) is simulated as the sum of the total photosynthesis of sunlit and shaded leaf groups (Chen et al., 1999):

$$A_{canopy} = A_{sun}(g_{sc,\,sun})L_{sun} + A_{sh}(g_{sc,sh})L_{sh} \quad (1)$$

where the subscripts "sun" and "sh" denote the sunlit and shaded components of the photosynthesis (A) and leaf area index (LAI or L). g_{sc} is the stomatal resistance for carbon molecules. The sunlit and shaded LAI are separated by (Chen et al., 1999; Norman, 1982):

$$L_{sun} = 2\cos\theta\left(1 - e^{-0.5\Omega L/\cos\theta}\right) \quad (2)$$

$$L_{sh} = L - L_{sun}$$

where θ is the solar zenith angle, Ω is the clumping index and L is the leaf area index. The net rate of CO_2 assimilation (either sunlit or shaded parts) is calculated as (Farquhar et al., 1980):

$$A = \min(A_c, A_j) - R_d \quad (3)$$

$$A_c = V_{cmax} f_V(T)\frac{C_i - \Gamma}{C_i + K_c(1 + O_i/K_o)} \quad (4)$$

$$A_j = J_{max} f_J(T)\frac{C_i - \Gamma}{2(C_i - 2\Gamma)} \quad (5)$$

where A,A_c, and A_j are the net photosynthetic, Rubisco-limited and light-limited gross photosynthetic rates $\mu mol\,m^{-2}\,s^{-1}$, respectively. R_d is the daytime leaf dark respiration, V_{cmax} is the maximum carboxylation rate at 25 °C. J_{max} is the electron transport rate at 25 °C. C_i and O_i are the intercellular CO_2 and oxygen concentration, respectively. Γ is the CO_2 compensation point without dark respiration, K_c and K_o are the Michaelis–Menten constants for CO_2 and oxygen respectively. $f_V(T)$ and $f_J(T)$ are the air temperature (T) response function for V_{cmax} and J_{max} respectively. In the model, the J_{max} is estimated from V_{cmax} (Medlyn et al., 1999):

$$J_{max} = 2.39 \times V_{cmax} - 14.2 \quad (6)$$

2.2. N-weighted V_{cmax} and $\boldsymbol{J_{max}}$ for sunlit and shaded leaves

The N-weighted V_{cmax} is derived according to Chen et al. (2012):

$$V_{cmax,sun} = V_{cmax,0} X_n N_0 \frac{k[1 - e^{-(k_n+k)L}]}{(k_n + k)(1 - e^{-kL})}$$
$$V_{cmax,sh} = V_{cmax,0} X_n N_0 \frac{1/k_n(1 - e^{-k_n L}) - \left(1 - e^{-(k_n+k)L}\right)\Omega/(k_n + k)}{L - 2\cos\theta(1 - e^{-kL})} \quad (7)$$

where $V_{cmax,0}$ is the leaf maximum Rubisco capacity at the top of the canopy at 25 °C, X_n is the ratio of measured Rubisco capacity to leaf N (Dai et al., 2004; dePury and Farquhar, 1997), N_0 is the N content at the top of the canopy; $k = G(\theta)\ \Omega/\cos\theta$, $G(\theta)$ is the projection coefficient, usually taken as 0.5 for spherical leaf angle distribution, k_n is the leaf N content decay rate with increasing depth into the canopy, taken as equal to 0.3 after dePury and Farquhar (1997).

2.3. Stomatal conductance

The leaf stomatal conductance g ($\mu mol\,m^{-2}\,s^{-1}$) is estimated from the photosynthesis rate A assuming that they are linearly related (Ball et al., 1987):

$$g = m\frac{Ah_s}{C_s} + b \quad (8)$$

where m is a plant species dependent coefficient. h_s and C_s are the relative humidity and CO_2 concentration at the leaf surface, respectively. b is the residual conductance. Eq. (8) is often called the Ball–Woodrow–Berry (BWB) equation. An analytical solution of g is used in our model in order to improve efficiency for global simulations (Baldocchi, 1994).

The important influences of soil water on g and A are not mechanistically included in the original BWB formulation (Eq. (8)). Following Bonan (1995) and Ju et al. (2006), we modify it as follows:

$$g = f_w\left(m\frac{Ah_s}{C_s}\right) + b \quad (9)$$

where f_w is a soil water stress factor, which we assume to be a function of soil water content and a unknown parameter to be optimized in this study. "$f_w\,m$" or "m (when $f_w = 1$)" also referred as the slope in the BWB equation in this paper.

2.4. Surface evaporation and canopy level transpiration

The latent heat (LE) is simulated as:

$$LE = \lambda(T + E_l + E_g) \quad (10)$$

where λ is the latent heat of vaporization. T is the transpiration rate from canopy ($kg\,m^{-2}\,s^{-1}$), E_l and E_g are evaporation rates of intercepted water from canopy and ground surface ($kg\,m^{-2}\,s^{-1}$), respectively.

The canopy level transpiration is obtained by:

$$T = T_{sun}(g_{s_{sun}})L_{sun} + T_{sh}(g_{s_{sh}})L_{sh} \quad (11)$$

where T_{sun} and T_{sh} are the average transpiration rates for sunlit and shaded leaves, respectively. g_s is stomatal resistance for water molecules. $g_s/g_{sc} = 1.6$. Following Wang and Leuning (1998), transpiration from sunlit leave is computed as (Ju et al., 2010):

$$T_{sun} = \frac{D_a + \Delta(T_{s,sun} - T_a)}{r_{sun}} \times \frac{\rho C_p}{\gamma} \quad (12)$$

where D_a is the atmospheric vapor pressure deficit (kPa). Δ is the rate of change of the saturated vapor pressure with temperature ($kPa\,°C^{-1}$). $T_{s,sun}$ and T_a are temperatures at sunlit leaf surface and air temperature (°C), respectively. ρ is the air density ($kg\,m^{-3}$). C_p is the specific heat of air at constant temperature ($1010\,J\,kg^{-1}\,°C^{-1}$), and

$$r_{sun} = r_b + r_a + \frac{1}{g_{s_{sun}}} \quad (13)$$

where r_a and r_b are aerodynamic and boundary layer resistance ($s\,m^{-1}$), respectively. And γ is the psychrometric constant ($kPa\,°C^{-1}$). To calculate T_{sh}, $T_{s,sh}$ (temperature at shaded leaf surface) and $g_{s_{sh}}$ are used to replace $T_{s,sun}$ and $g_{s_{sun}}$ in Eqs. (12) and (13).

The evaporation from intercepted water from sunlit and shaded leave E_l are estimated similarly using Eqs. (11) –(13), but without the term for stomatal resistance (i.e., $r_s = 0$).

The evaporation from soil E_g is estimated using the Penman–Monteith equation (Monteith, 1965):

$$\lambda E_g = \frac{\Delta(R_g - 0) + \rho C_p VPD_g/r_{a_g}}{\Delta + \gamma(1 + r_{soil}/r_{a_g})} \quad (14)$$

where R_g is the net radiation in the ground, VPDg is vapor pressure deficit at the ground level, r_{a_g} is the aerodynamic resistance of ground surface, r_{soil} is the soil resistance for evaporation. In Sellers et al. (1996),

$$r_{soil} = \exp\left(8.2 - 4.2 \times \frac{\theta_1}{\theta_s}\right) \quad (15)$$

where θ_1 is volumetric soil VWC in first layer ($m^3\,m^{-3}$), and θ_s is value of θ at saturation ($m^3\,m^{-3}$). The r_{soil} from Sellers et al. (1996) is a rough estimate and we used $4 \times r_{soil}$ in the BEPS model.

2.5. Parameter optimization

The Kalman filter (KF) is a variance-minimizing algorithm that updates the state estimate whenever measurements are available (Evensen, 2009). The cost function for KF is written as:

$$J = (X_k^a - X_k^f)^T P^{-1}(X_k^a - X_k^f) + \left(Y_k - H(X_k^f)\right)^T R^{-1}\left(Y_k - H(X_k^f)\right) \quad (16)$$

where X_k^a and X_k^f are the analyzed and forecast estimates respectively, at time instant k , Y_k is the vector of measurements, H is the measurement operator that maps the model state X_k–Y_k, P is the error covariance of the predicted model state, and R is the measurement error covariance matrix. Minimizing with respect to X_k^a yields the KF update equation:

$$X_k^a = X_k^f + K\left(Y_k - H(X_k^f)\right) \quad (17)$$

$$K = P_k^f H^T (H P_k^f H^T + R_k)^{-1} \quad (18)$$

where $P_k^f H^T$ is the cross covariance between any given state and prediction, $H\left(X_k^f\right)$ for an ensemble Kalman filter (EnKF),

$$P_k^f H^T = \frac{X_k^f - \overline{X}_k^f}{u - 1} q_k^T \quad (19)$$

$$q_k^d = H(X_k^f - \overline{X}_k^f) = (y_k^f - \overline{y}_k^f) \quad (20)$$

where y are individual ensemble member of the prediction, $HP_k^f H^T$ is the error covariance matrix of the prediction,

$$P_k^f = \frac{(X_k^f - \overline{X}_k^f)(X_k^f - \overline{X}_k^f)^T}{u - 1} \quad (21)$$

Table 1
The initial values, standard deviations, and ranges of the two parameters optimized.

	Symbol	Unit	Initial value	Standard deviation	Range
Step 1	V_{cmax}	$\mu mol\ m^{-2}\ s^{-1}$	10	3.0, 1.0[a]	5–∞
	f_w	dimensionless	1	0.1	0.01–∞
Step 2	V_{cmax}	$\mu mol\ m^{-2}\ s^{-1}$	10	3.0, 1.0[a]	5–∞
Step 3	f_w	dimensionless	1	0.1	0.01–∞

[a] 3.0 for leaf expansion stage, 1.0 for other stages.

$$HP_k^f H^T = \frac{q_k q_k^T}{u-1} \quad (22)$$

u is the ensemble number.

The EnKF is applied to optimize two key parameters of the BEPS model: f_w (Section 2.3, Eq. (9)) and the leaf level V_{cmax} at the top of the canopy at 25 °C (the $V_{cmax,0}$ in Section 2.2, Eq. (7), referred to as V_{cmax} hereafter). The analysis is limited to rain-free days. These parameters are optimized through assimilating observations of latent heat (LE) and gross primary productivity (GPP) fluxes measured at flux tower sites. The optimization is conducted daily. Observational errors for the daily GPP and LE fluxes are set to 15% following previous studies (Ju et al., 2010; Mo et al., 2008), and the cross-correlations of LE and GPP fluxes errors are assumed to be negligible (Lasslop et al., 2008). The ensemble size is set to 100 (Mo et al., 2008).

We developed a three-step scheme to optimize the two parameters in different temporal scales. The configurations of the EnKF for the three steps are listed in Table 1. To ensure enough spread of the ensemble, we set different perturbations for the early growing season and for subsequent seasons, based on several experiments. To prevent filter divergence (Ng et al., 2011), the BEPS model was reinitialized to generate a new ensemble after each DA. In all three steps, both measured LE and GPP fluxes are used in the DA. First, the EnKF is applied daily to obtain precursor estimates of V_{cmax} and f_w. Then V_{cmax} is optimized at different time scales (1–15 days in step of 2 days) assuming f_w is unchanged from the first step by re- running the EnKF. In this step, the observational errors for LE and GPP in a window are estimated as $15\%/\sqrt{days}$. The best temporal period or window size is then determined by analyzing the magnitude of the minimized cost-function, and the coefficient of determination (R^2) and root-mean- square deviation (RMSE) of LE and GPP between simulation and observation. Finally, the daily f_w value is optimized for rain free days corresponding to the V_{cmax} curve from the best window size by re-running EnKF. The optimized f_w is then compared with shallow soil VWC in second layer as shown in Table 2.

In this study we follow the idea that the f_w affects the slope of the BWB equation, and we assume that there would be a sudden change in f_w right after a precipitation event (Fig. 1). Though the BEPS model has a module to predict f_w, we do not use it to provide *a priori* in the EnKF. So in the EnKF, it is unreasonable to use the f_w before rain for the *a priori* estimate of f_w after rain (Fig. 1b) because the use of f_w before the rain event would introduce or enhance the "time lag" between the analysis and the true state. In areas where rain events are very frequent, estimates of f_w are unreliable. To solve this problem, we reinitialize the EnKF to produce a new *a priori* estimate of f_w after rain events, assuming that the $f_w = VWC \times 8.0$ based on several experiments, where VWC is for the second soil layer (Fig. 1b and c). The problem of optimization of the f_w then turns into a test if the optimized f_w will deviate from the yellow long dash line (representing a linear trend) after a rain event. In the early growth season, we examine if the f_w will be significantly below the yellow long dash line (in Fig. 1c) when the soil water content is abundant. If it is, we will not reinitialize the f_w after rain events and just use the f_w optimized from previous day in order to test the effect of soil temperature.

2.6. Data

We tested the EnKF scheme for three flux tower sites for year 2009: (1) a 74 year-old white pine forest, which is part of the Turkey Point Flux Station's age- sequence sites (TP39) in southern Ontario, Canada (Peichl et al., 2010), (2) an old jack pine (OJP) site in the southern area of the boreal ecosystem-atmosphere study

Table 2
Site information about the three flux tower sites.

Site	White pine (TP39)	Old aspen (OA)	Old jack pine (OJP)
	(Pinus strobes L.*)*	*(Populus tremuloides Michx)*	*(Pinus banksiana)*
Location	42.71°, −80.36°	53.63°, −106.20°	53.92°, −104.69°
Sapling year	1939	1919	1914
Overstory	Mature white pine (*P. strobus*)	Trembling aspen (Populus *tremuloides Michx*)	Mature jack pine (*Pinus Banksiana*)
Understory	*Q. vultina*, Abies balsamifera, *Prunus serotina*	Hazelnut	Very sparse green alder (predominantly lichen ground cover)
Forest type	Evergreen needle leaf	Deciduous forest	Evergreen needle leaf
Maximum LAI	~8 (overstory)	4.5 (total)	2.82 (overstory)
Clumping index	0.65	0.68	0.51
Soil type	Sandy loam	Silt loam	Sandy
Elevation (m)	219	580	579.27
Topography	Flat land	Generally level	Undulating
Mean annual air temperature (°C)	8.3 (2009)	0.5	0.4
Mean annual precipitation (mm)	860 (2009)	406	467.2
Organic layer depth (cm)	4	2–4	8–10
Soil water content layer (cm)	0–5, 5–10, 10–20, 20–50, 50–100	0–5, 5–15, 15–30, 30–60, 60–120	0–15, 15–30, 30–60, 60–90, 90–120, 120–150
Tree heights (m)	22	24.1	16.7

References: (Arain et al., 2002; Arain and Restrepo-Coupe, 2005; Arain et al., 2006; Barr et al., 2004; Black et al., 1996; Chen et al., 2007; Chen et al., 2006; Chen et al., 1997; Cuenca et al., 1997; He et al., 2012; Ju et al., 2006; Mo et al., 2008; Peichl et al., 2010).

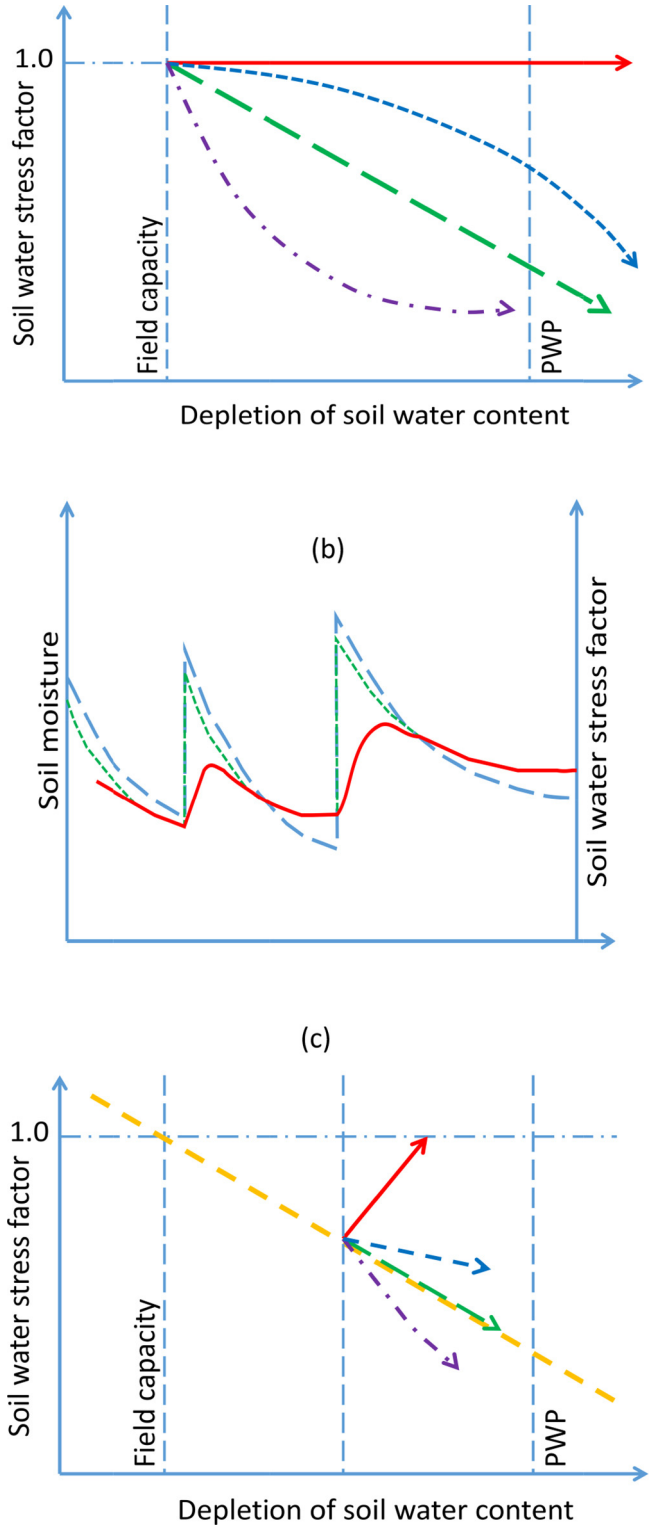

Fig. 1. Testing scheme for soil water stress. (a) the soil water stress on plant (f_w) can be constant (red solid line), linear (long green dash line), or other unknown forms (blue dash or purple dot dash) along with the depletion of soil water content from field capacity to permanent wilting point (PWP); (b) soil water content is shown in the long dash blue line. The assumed true response of f_w to soil water content after a rain is in short green dash line. The red solid line indicates f_w with an incorrect time-lag caused by the analysis process in the EnKF. (c) f_w is reinitialized in the EnKF after each rain using value in the long yellow dash line; the direction of vector (optimized f_w) shows whether f_w is departing from the yellow line, a linear hypothesis. (For interpretation of the references to color in this figure legend, the reader is referred to the web version of this article.)

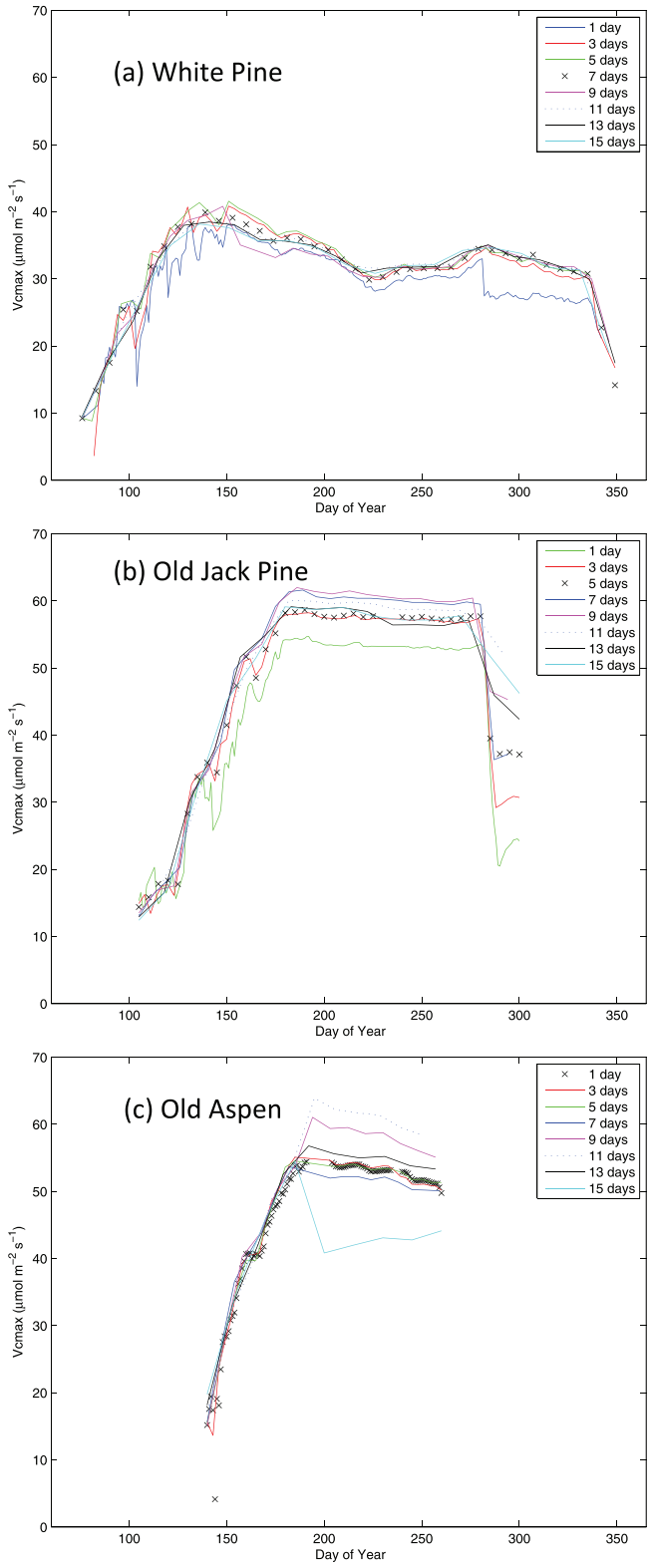

Fig. 2. The seasonal variations of V_{cmax} for different time-windows at three sites: (a) TP39 site, (b) OJP site, and (c) OA site in 2009. (For interpretation of the references to color in this figure legend, the reader is referred to the web version of this article.)

(BOREAS), Saskatchewan, Canada (Black et al., 1996; Chen et al., 2007), and (3) an old aspen site in the southern BOREAS (OA) (Barr et al., 2004; Ju et al., 2006). The key parameters are summarized in the Table 2.

Table 3
Coefficient of determination (R^2) and root-mean-square deviation (RMSE) between optimized fluxes and their measurements for the Turkey Point (TP39) site.

	Window (days)	GPP_h R^2	GPP_h RMSE ($g C m^{-2} h^{-1}$)	LH_h R^2	LH_h RMSE ($W m^{-2}$)	Median J
Step 1	1	0.773	0.123	0.761	35.56	4.49
	1	0.78	0.122	0.775	31.90	3.86
	3	0.785	0.126	0.776	32.32	5.01
	5	0.782	0.129	0.776	32.57	5.10
Step 2	7	0.783	0.127	0.777	31.79	5.02
	9	0.785	0.124	0.776	31.54	5.02
	11	0.78	0.13	0.774	32.35	5.02
	13	0.773	0.133	0.775	31.74	5.01
	15	0.768	0.134	0.775	31.80	5.01
Step 3	7	0.786	0.122	0.764	35.88	3.68

Note: GPP_h and LH_h are for half hourly GPP and latent heat, respectively. J is the value of cost function. The three significant digits for R^2 and RMSE are used to shown the effect of window sizes in DA.

Table 4
Coefficient of determination (R2) and root-mean-square deviation (RMSE) between optimized fluxes and their measurements for the old jack pine (OJP) site.

	Window (days)	GPP_h R^2	GPP_h RMSE($g C m^{-2} h^{-1}$)	LH_h R^2	LH_h RMSE($W m^{-2}$)	Median J
Step 1	1	0.688	0.072	0.617	25.99	7.65
	1	0.703	0.076	0.628	25.29	6.89
	3	0.715	0.078	0.631	25.61	8.60
	5	0.709	0.079	0.635	25.28	9.27
Step 2	7	0.710	0.082	0.633	25.92	8.78
	9	0.704	0.083	0.634	25.76	8.99
	11	0.703	0.083	0.629	25.71	8.60
	13	0.698	0.826	0.632	25.04	8.60
	15	0.692	0.084	0.633	24.81	8.54
Step 3	7	0.692	0.084	0.616	28.81	6.31

Note: GPP_h and LH_h are for half hourly GPP and latent heat, respectively.

Half-hourly measurements of meteorological variables (air temperature, incoming solar radiation, relative humidity, and wind speed), leaf area index (LAI), and clumping index from ground measurement or remote sensing are used to drive the BEPS model in half-hourly step, and energy (LE) and CO_2 (GPP) fluxes using eddy covariance technique are used to constrain the model in the EnKF. For the OA site, the LAI is collected from work by Barr et al. (2004) using the gap-filling approach; for TP39 site, the LAI is measured by tracing radiation and architecture of canopies (TRAC) instrument and LAI2000; for the OJP site, remote sensed LAI curve from MODIS is adjusted to match 2/3 to 1 of the maximum LAI from TRAC according to Jack pine's leaf turnover rate. The upper soil VWC measurement is used in the calculation of soil surface resistance, and the soil VWC measurement in the second layer is used to initialize f_w after rain events and as an independent variable to compare with optimized f_w.

3. Results

3.1. The optimal time window for determining V_{cmax} temporal variability

The seasonal variations of optimized V_{cmax} are shown in Fig. 2 for the three sites in 2009, for different time window sizes. As expected, the window size has an effect on the shape of optimized V_{cmax}, with smaller windows leading to noisier curves and bigger

Table 5
Coefficient of determination (R2) and root-mean-square deviation (RMSE) between optimized fluxes and their measurements for the old aspen (OA) site.

	Window (days)	GPP_h R^2	GPP_h RMSE($g C m^{-2} h^{-1}$)	LH_h R^2	LH_h RMSE($W m^{-2}$)	Median J
Step 1	1	0.81	0.162	0.736	56.62	3.86
	1	0.83	0.16	0.718	55.49	4.41
	3	0.831	0.161	0.716	55.35	5.47
	5	0.828	0.162	0.712	55.31	5.44
Step 2	7	0.819	0.165	0.711	54.76	5.44
	9	0.805	0.184	0.712	56.53	5.83
	11	0.8	0.19	0.714	56.19	5.44
	13	0.798	0.181	0.705	55.41	5.47
	15	0.791	0.167	0.696	52.01	4.65
Step 3	7	0.814	0.166	0.734	57.72	3.74

Note: GPP_h and LH_h are for half hourly GPP and latent heat, respectively.

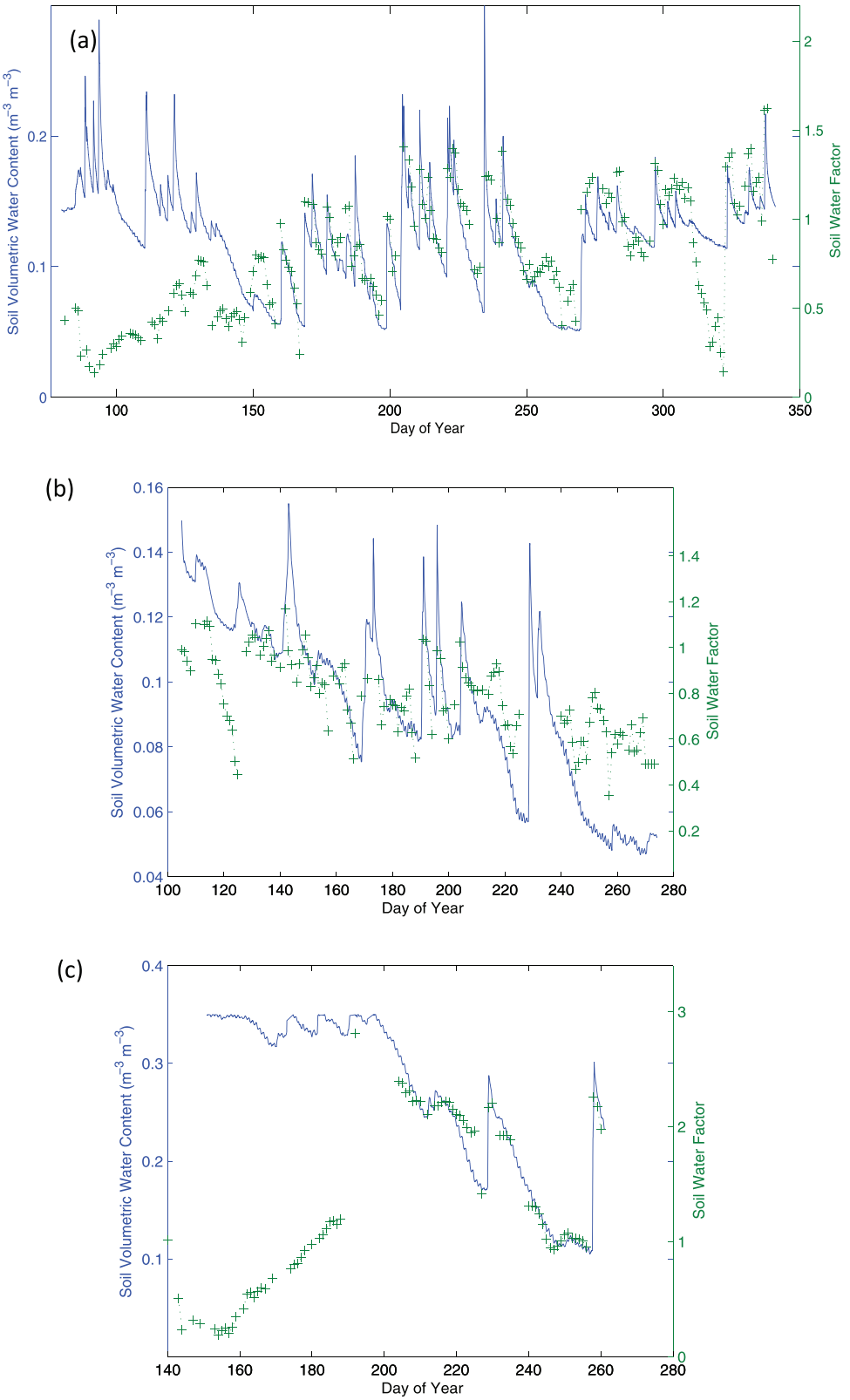

Fig. 3. The soil water stress factor (f_w) vs. soil volumetric water content (VWC) at the three sites: (a) TP39 site, (b) OJP site, and (c) OA site. Blue soild line is for soil VWC, and green plus marker is for optimized f_w. (For interpretation of the references to color in this figure legend, the reader is referred to the web version of this article.)

windows to smoother curves (Fig. 2). The large difference in V_{cmax} after DOY 280 in Fig. 2b is caused by incomplete time windows at the end of the growing season. The separate asymptotes of V_{cmax} after DOY 190 in Fig. 2c are artifacts caused by a data gap. As shown in Tables 3–5, smaller windows generally lead to smaller RMSE or larger R^2 for the GPP for all sites. In contrast, the maximum R^2 for LE at two of the sites occurred in medium-sized windows (7 days for TP39, and 5 days for OJP) with OA as an exception (1 day). From a

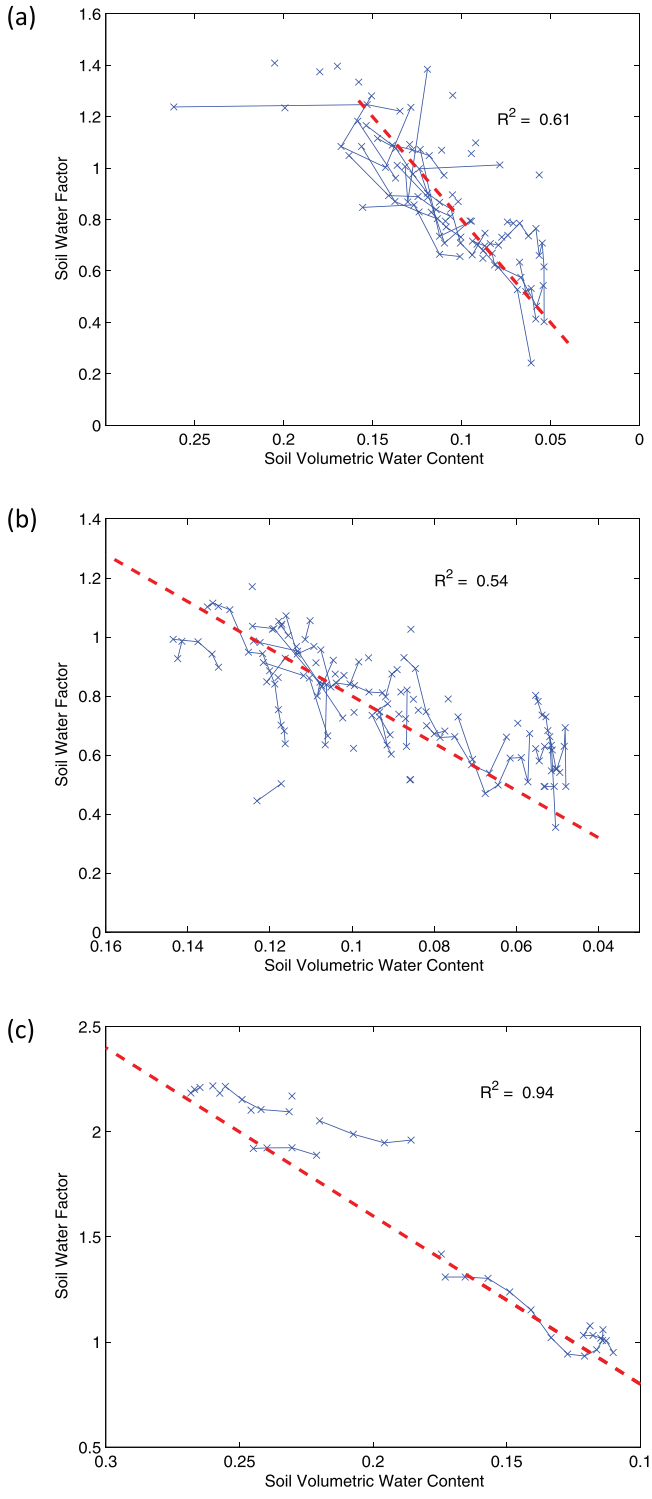

Fig. 4. The scattering plots of soil water stress factor (f_w) and soil VWC in the summer at (a) TP39 site, (b) OJP site, and (c) OA site. In each plot the red-dash line shows $f_w = 8 \times$ VWC which is used for initialized value after rain. The connected markers are for optimized values for continuous days within two rain events with f_w being initialized after the rain from the red-dash line. The separated markers are from short periods or from long periods being separated by failed optimizations. (For interpretation of the references to color in this figure legend, the reader is referred to the web version of this article.)

biological point of view, the smoother V_{cmax} curve from the larger window in LE simulation may be more realistic than the less smooth V_{cmax} curve from the 1-day window, even though the R^2 of GPP of the larger window is not the maximum. It is conceivable that smaller window sizes mathematically give larger flexibility for the model to fit GPP measurements, inducing larger R^2 values, and therefore the optimized parameters contain some mathematical artifacts. For the same reason, mathematical artifacts could also influence the model fit to LE data. In the BEPS model, V_{cmax} influences LE through its influence on stomatal conductance. With f_w given the full freedom to modify the LE calculation through adjusting the stomatal conductance, the influence of V_{cmax} is much weaker on LE than on GPP. Under this mathematical setting, V_{cmax} is optimized based on the remainder of the LE variance that is not explained by f_w and generally has temporal scales longer than the time step used in the optimization. We therefore believe that the optimal time window for V_{cmax} optimization found based on LE simulation captures the realistic temporal variability of V_{cmax}, although such temporal variability signals are not always strong in our optimization procedure.

3.2. Seasonal variations of the V_{cmax}

Generally, all V_{cmax} values at these sites increase rapidly at the beginning of leaf emergence (OA site) or greenness (TP39 and OJP sites), and reach their peaks in late spring or early summer. They decline in the fall with leaf senescence and/or breakdown of leaf chlorophyll. There are also small fluctuations in V_{cmax} that may be imposed by soil water stress in summer (Bertrand and Schoefs, 1999; Misson et al., 2006; Wilson et al., 2000) and/or low air temperature in the spring.

Following the results from the optimal window, the peak values of V_{cmax} are approximately 40, 57, and 54 $\mu mol\,m^{-2}\,s^{-1}$ for the TP39, OJP, and OA sites, respectively. The dates to reach peak of V_{cmax} differ with the sites' mean annual air temperatures: at ~140 DOY for TP39 site, at ~180 DOY for the OJP site, and at ~190 DOY for the OA site. For the TP39 site (Fig. 2a), there is a decline of the V_{cmax} curve in the mid-summer associated with the drought. Of the three sites, the OA site is a deciduous forest and it is notable for the short growing season with later leaf emergence shown from the V_{cmax} curve (Fig. 2c).

We noticed the rapid decrease of the optimized V_{cmax} in the fall. However, we restrain further comments due to the unreliable LAI gap-filled method in the fall (Barr et al., 2004) and breakdown of leaf chlorophyll, which make the optimization less confident.

3.3. Soil water stress and the slope of BWB equation

The optimized f_w along with the soil VWC in the 2nd layer (5–10, 5–15, and 15–30 cm for the TP39, OA, and OJP sites, respectively) for the three sites are shown in Fig. 3. Since the m values for the three sites in the BWB equation are all fixed at a value of 8 during the optimization and the m values might be species dependent, it is possible that f_w can be larger than one if the m value is too small. The actual slope of BWB equation equals to the product of f_w and m.

We found that the optimized f_w values in the summer have large variations and the variations can be largely explained by the VWC (Fig. 4) in the 2nd layer. The optimized f_w ranges from ~0.3 to ~1.4 at TP39 (Fig. 4a). It is very stable and close to 1.3 when the VWC is above the field capacity (0.16) (Peichl et al., 2010). For the OJP site, f_w ranges from ~0.5 to ~1.1; when the shallow (15–30 cm) VWC is close to the permanent wilting point (PWP) (~0.05 for sand), it does not continually decrease with the depletion of soil water content, implying that trees might make use of soil water in the deeper layers (Fig. 4b). For the OA site, f_w ranges from ~1.0 to ~2.2 in the summer, meaning that the m can be as high as 17.6 at this site (Fig. 4c). Comparing to TP39 and OJP (both sandy soil), the

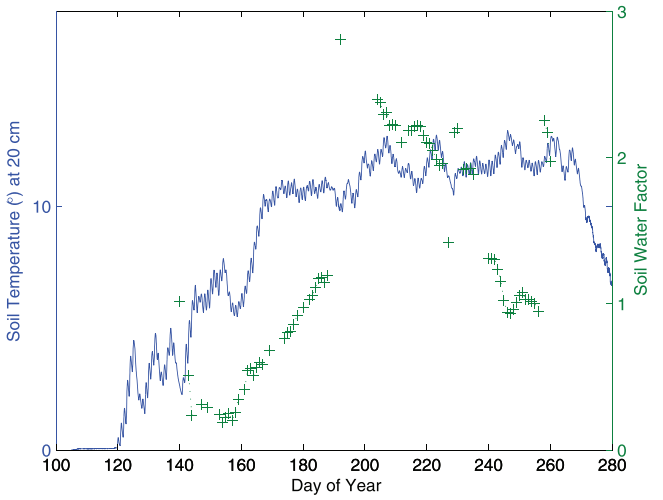

Fig. 5. The relationship between soil water stress factor (f_w, green plus) and soil temperature (blue line) in the second layer for OA site. (For interpretation of the references to color in this figure legend, the reader is referred to the web version of this article.)

loam soil in OA has a smaller hydraulic conductivity and a higher available water capacity, so VWC and f_w change slowly.

3.4. Stress due to soil temperature

In the spring, f_w has a different trend with the VWC change. We intentionally show an example in Fig. 3b where the optimized f_w drops to a much lower value (~0.3) than the initialized value of 1.0, when the soil water content is abundant (before DOY ~120), implying that there is another stress in addition to soil water content. Consequently, in the spring we did not reinitialize the f_w after rain in the EnKF for the TP39 and OA sites. For the TP39 site, f_w increases from 0.2 to 0.7 between DOY 80–130 (Fig. 3a). For the OA site (Fig. 3c), f_w increases smoothly from ~0.2 to 1.0 between DOY 150–190.

We examined the f_w – soil temperature relationship in Fig. 5 for the OA site. In the seasonal trend, f_w increases with soil temperature in the spring when the soil water content is abundant, but f_w does not change sensitively with soil temperature, e.g., around DOY 160, f_w does not decrease as the soil temperature decreases.

In the fall and winter, there is still stress due to temperature shown in f_w for the TP39 site even when soil water content is abundant, e.g., DOY ~320 and later.

4. Discussion

4.1. Errors in model structure, other parameters, and driving data

The optimization is prone to errors in model structures and others fixed parameters, driving or forcing data, and the observations (Carvalhais et al., 2008). Essentially the optimized parameters include projections of all the uncertainties and variations from the model-data assimilation approach on the optimized parameters.

In this study, only two parameters (V_{cmax} and f_w) are optimized, corresponding to the two independent observations (GPP and LE). However, other parameters may also have contributed to the variations in GPP and LE. For example, errors in LAI variation can be mapped into V_{cmax}, and uncertainty in soil surface evaporation can be mapped into f_w.

In this study, we are aware of the importance of the temporal scales of parameters in EnKF. V_{cmax} changes at a temporal scale of few days to few weeks while f_w can change in few minutes to few hours. To minimize the possibility that other short term variations may be mapped into V_{cmax} we have proposed a three-stage approach for optimization. To reduce the mathematical artifact in the derived curves, we also used smaller spreads of V_{cmax} in the late growth seasons than in spring, so it is also possible that the real variations of the V_{cmax} in these seasons are smoothed. Further study is needed to address the temporal variations of the V_{cmax}.

4.2. The variation of f_w

Our results generally support the assumption that the slope in the BWB equation is not constant and depends on vegetation species. The values of m generally fall in the range of previous studies (Heroult et al., 2013; Ju et al., 2010; Medlyn et al., 2011; Mo et al., 2008; Wolf et al., 2006). We found that f_w is generally linearly related to VWC in the summer. When the soil VWC is very close to the field capacity and PWP, f_w departs from the linear relationship. Therefore, it is more physically reasonable to model f_w using soil water suction/potential than using soil VWC. The calculation of soil water suction generally needs four parameters for each layer (Chen et al., 2007). While these parameters are usually unavailable in the regional and global scales, the linear relationship would be a practically useful approximation.

It is shown from Fig. 5 that f_w gradually increases with soil temperature during the spring when the soil VWC is abundant, but f_w does not follow tightly with soil temperature, e.g., from DOY of around 160, f_w does not decrease when the soil temperature decreases. Low soil temperature has been shown to inhibit the growth of fine roots (Burke and Raynal, 1994; Côté et al., 1998; Deans, 1979; Lahti et al., 2005; Mainiero et al., 2010; Pregitzer et al., 2000). Therefore, we propose that the stress in f_w in the spring is from the limited amount of fine roots in the early growing season.

5. Conclusion

Using an EnKF approach, we optimized seasonal variations of two important and commonly used parameters in ecosystem models: the maximum photosynthetic carboxylation rate at 25 °C (V_{cmax}), and the soil water stress factor (f_w). The former regulates the photosynthesis process; the latter affects carbon–water coupling thus influencing both photosynthesis and transpiration. This study quantifies the seasonal variations in V_{cmax} and f_w, which are usually not taken into consideration in ecosystem models. The importance of different temporal scales in parameter optimization needs further investigation. Significant variations of these two parameters with season as well as with forest type imply that further improvements in model parameterization are needed. In spite of uncertainties in the optimization, following conclusions can be drawn:

(1) Based on the BEPS model structure, our optimization supports a variable slope (proportional to f_w) in the Ball–Berry–Woodrow equation. Furthermore, the variation of the slope is largely explained by the soil water content in the shallow layer in the summer. The slope is not sensitive to the soil water content in shallow layer, when soil VWC is close to permanent wilting point, implying that the plant can still uptake water from deeper layers during drought.
(2) In the early and late growing season, the variation in f_w cannot be explained by soil water content alone. In the early spring, f_w gradually increases with soil temperature, suggesting that the fine root development with increasing temperature may be the main reason for the f_w increasing trend. In the fall, f_w decreases

with decreasing temperature, and this is also likely caused by the fine-root mortality. These results suggest the importance in considering fine root development and mortality processes in modeling ecosystem water and carbon cycling.

(3) There is a rapid increase of V_{cmax} in the early growing season. In the summer, the variation of V_{cmax} becomes smaller.

Acknowledgements

This work was supported by the Canadian Space Agency grant (11SUSMAPTO). We would like to acknowledge the investigators of the Boreal Ecosystem-Atmosphere Study (BOREAS) project and the Fluxnet Canada project for the various data sets used in this study: Harry McCaughey (Queen's University), and T. Andrew Black (University of British Columbia). We also acknowledge numerous researchers and students involved in collecting data sets at Turkey Point Flux Station. The authors would like to thank two anonymous reviewers whose constructive comments led to a better presentation of our research methods and results.

References

Arain, M.A., Black, T.A., Barr, A.G., Jarvis, P.G., Massheder, J.M., Verseghy, D.L., Nesic, Z., 2002. Effects of seasonal and interannual climate variability on net ecosystem productivity of boreal deciduous and conifer forests. Can. J. For. Res. 32, 878–891.

Arain, M.A., Restrepo-Coupe, N., 2005. Net ecosystem production in a temperate pine plantation in southeastern Canada. Agric. For. Meteorol. 128, 223–241.

Arain, M.A., Yuan, F.M., Black, T.A., 2006. Soil-plant nitrogen cycling modulated carbon exchanges in a western temperate conifer forest in Canada. Agric. For. Meteorol. 140, 171–192.

Baldocchi, D., 1994. An analytical solution for coupled leaf photosynthesis and stomatal conductance models. Tree Physiol. 14, 1069–1079.

Ball, J., Woodrow, L.E., Beny, J.A., 1987. A model predicting stomatal conductance and its contribution to the control of photosynthesis under different environmental conditions. In: Biggins, J. (Ed.), Progress in Photosynthesis Research, vol 4. Nijhoff, Dordrecht, pp. 221–224.

Barr, A.G., Black, T.A., Hogg, E.H., Kljun, N., Morgenstern, K., Nesic, Z., 2004. Inter-annual variability in the leaf area index of a boreal aspen-hazelnut forest in relation to net ecosystem production. Agric. For. Meteorol. 126, 237–255.

Bertrand, M., Schoefs, B., 1999. Photosynthetic pigment metabolism in plants during stress, In: Pessarakli, M. (Ed.), Handbook of Plant and Crop Stress. second ed. CRC Press, 527-543.

Black, T.A., DenHartog, G., Neumann, H.H., Blanken, P.D., Yang, P.C., Russell, C., Nesic, Z., Lee, X., Chen, S.G., Staebler, R., Novak, M.D., 1996. Annual cycles of water vapour and carbon dioxide fluxes in and above a boreal aspen forest. Global Change Biol. 2, 219–229.

Bonan, G.B., 1995. Land atmosphere CO_2 exchange simulated by a land-surface process model coupled to an atmospheric general-circulation model. J. Geophys. Res. 100, 2817–2831.

Burke, M., Raynal, D., 1994. Fine root growth phenology, production, and turnover in a northern hardwood forest ecosystem. Plant Soil 162, 135–146.

Cai, T.B., Dang, Q.L., 2002. Effects of soil temperature on parameters of a coupled photosynthesis-stomatal conductance model. Tree Physiol. 22, 819–827.

Carvalhais, N., Reichstein, M., Seixas, J., Collatz, G.J., Pereira, J.S., Berbigier, P., Carrara, A., Granier, A., Montagnani, L., Papale, D., Rambal, S., Sanz, M.J., Valentini, R., 2008. Implications of the carbon cycle steady state assumption for biogeochemical modeling performance and inverse parameter retrieval. Global Biogeochem. Cycles 22, GB2007.

Chen, B., Chen, J.M., Ju, W., 2007. Remote sensing-based ecosystem-atmosphere simulation scheme (EASS) – model formulation and test with multiple-year data. Ecol. Modell. 209, 277–300.

Chen, J.M., Govind, A., Sonnentag, O., Zhang, Y.Q., Barr, A., Amiro, B., 2006. Leaf area index measurements at Fluxnet-Canada forest sites. Agric. For. Meteorol. 140, 257–268.

Chen, J.M., Liu, J., Cihlar, J., Goulden, M.L., 1999. Daily canopy photosynthesis model through temporal and spatial scaling for remote sensing applications. Ecol. Modell. 124, 99–119.

Chen, J.M., Mo, G., Pisek, J., Liu, J., Deng, F., Ishizawa, M., Chan, D., 2012. Effects of foliage clumping on the estimation of global terrestrial gross primary productivity. Global Biogeochem. Cycles 26.

Chen, J.M., Rich, P.M., Gower, S.T., Norman, J.M., Plummer, S., 1997. Leaf area index of boreal forests: theory, techniques, and measurements. J. Geophys. Res. 102, 9–29443.

Côté, B., Hendershot, W., Fyles, J., Roy, A., Bradley, R., Biron, P., Courchesne, F., 1998. The phenology of fine root growth in a maple-dominated ecosystem: relationships with some soil properties. Plant Soil 201, 59–69.

Cuenca, R.H., Stangel, D.E., Kelly, S.F., 1997. Soil water balance in a boreal forest. J. Geophys. Res. 102, 29355–29365.

Dai, Y.J., Dickinson, R.E., Wang, Y.P., 2004. A two-big-leaf model for canopy temperature, photosynthesis, and stomatal conductance. J. Clim. 17, 2281–2299.

Deans, J.D., 1979. Fluctuations of the soil environment and fine root growth in a young Sitka spruce plantation. Plant Soil 52, 195–208.

dePury, D.G.G., Farquhar, G.D., 1997. Simple scaling of photosynthesis from leaves to canopies without the errors of big-leaf models. Plant Cell Environ. 20, 537–557.

Dietze, M.C., Vargas, R., Richardson, A.D., Stoy, P.C., Barr, A.G., Anderson, R.S., Arain, M.A., Baker, I.T., Black, T.A., Chen, J.M., Ciais, P., Flanagan, L.B., Gough, C.M., Grant, R.F., Hollinger, D., Izaurralde, R.C., Kucharik, C.J., Lafleur, P., Liu, S.G., Lokupitiya, E., Luo, Y.Q., Munger, J.W., Peng, C.H., Poulter, B., Price, D.T., Ricciuto, D.M., Riley, W.J., Sahoo, A.K., Schaefer, K., Suyker, A.E., Tian, H.Q., Tonitto, C., Verbeeck, H., Verma, S.B., Wang, W.F., Weng, E.S., 2011. Characterizing the performance of ecosystem models across time scales: a spectral analysis of the North American Carbon Program site-level synthesis. J. Geophys. Res. Biogeosci. 116.

Evensen, G., 2009. The ensemble Kalman filter for combined state and parameter estimation Monte Carlo techniques for data assimilation in large systems. IEEE Control Syst. Mag. 29, 83–104.

Farquhar, G.D., Caemmerer, S.V., Berry, J.A., 1980. A biochemical-model of photosynthetic CO_2 assimilation in leaves of C-3 species. Planta 149, 78–90.

Grassi, G., Magnani, F., 2005. Stomatal, mesophyll conductance and biochemical limitations to photosynthesis as affected by drought and leaf ontogeny in ash and oak trees. Plant Cell Environ. 28, 834–849.

Grassi, G., Vicinelli, E., Ponti, F., Cantoni, L., Magnani, F., 2005. Seasonal and interannual variability of photosynthetic capacity in relation to leaf nitrogen in a deciduous forest plantation in northern Italy. Tree Physiol. 25, 349–360.

He, L.M., Chen, J.M., Pisek, J., Schaaf, C.B., Strahler, A.H., 2012. Global clumping index map derived from the MODIS BRDF product. Remote Sens. Environ. 119, 118–130.

Heroult, A., Lin, Y.S., Bourne, A., Medlyn, B.E., Ellsworth, D.S., 2013. Optimal stomatal conductance in relation to photosynthesis in climatically contrasting Eucalyptus species under drought. Plant Cell Environ. 36, 262–274.

Houborg, R., Cescatti, A., Migliavacca, M., Kustas, W.P., 2013. Satellite retrievals of leaf chlorophyll and photosynthetic capacity for improved modeling of GPP. Agric. For. Meteorol. 177, 10–23.

Jensen, R.G., 2000. Activation of Rubisco regulates photosynthesis at high temperature and CO_2. Proc. Natl. Acad. Sci. U. S. A. 97, 12937–12938.

Ju, W., Chen, J.M., Black, T.A., Barr, A.G., Liu, J., Chen, B., 2006. Modelling multi-year coupled carbon and water fluxes in a boreal aspen forest. Agric. For. Meteorol. 140, 136–151.

Ju, W., Wang, S., Yu, G., Zhou, Y., Wang, H., 2010. Modeling the impact of drought on canopy carbon and water fluxes for a subtropical evergreen coniferous plantation in southern China through parameter optimization using an ensemble Kalman filter. Biogeosciences 7, 845–857.

Kattge, J., Knorr, W., Raddatz, T., Wirth, C., 2009. Quantifying photosynthetic capacity and its relationship to leaf nitrogen content for global-scale terrestrial biosphere models. Global Change Biol. 15, 976–991.

Keenan, T., Garcia, R., Friend, A.D., Zaehle, S., Gracia, C., Sabate, S., 2009. Improved understanding of drought controls on seasonal variation in Mediterranean forest canopy CO_2 and water fluxes through combined in situ measurements and ecosystem modelling. Biogeosciences 6, 1423–1444.

Keenan, T., Sabate, S., Gracia, C., 2010a. The importance of mesophyll conductance in regulating forest ecosystem productivity during drought periods. Global Change Biol. 16, 1019–1034.

Keenan, T., Sabate, S., Gracia, C., 2010b. Soil water stress and coupled photosynthesis-conductance models: Bridging the gap between conflicting reports on the relative roles of stomatal, mesophyll conductance and biochemical limitations to photosynthesis. Agric. For. Meteorol. 150, 443–453.

Lahti, M., Aphalo, P.J., Finér, L., Ryyppö, A., Lehto, T., Mannerkoski, H., 2005. Effects of soil temperature on shoot and root growth and nutrient uptake of 5-year-old Norway spruce seedlings. Tree Physiol. 25, 115–122.

Lasslop, G., Reichstein, M., Kattge, J., Papale, D., 2008. Influences of observation errors in eddy flux data on inverse model parameter estimation. Biogeosciences 5, 1311–1324.

Liu, Y., Weerts, A.H., Clark, M., Franssen, H.J.H., Kumar, S., Moradkhani, H., Seo, D.J., Schwanenberg, D., Smith, P., van Dijk, A.I.J.M., van Velzen, N., He, M., Lee, H., Noh, S.J., Rakovec, O., Restrepo, P., 2012. Advancing data assimilation in operational hydrologic forecasting: progresses, challenges, and emerging opportunities. Hydrol. Earth Syst. Sci. 16, 3863–3887.

Mainiero, R., Kazda, M., Schmid, I., 2010. Fine root dynamics in 60-year-old stands of *Fagus sylvatica* and *Picea* abies growing on haplic luvisol soil. Eur. J. For. Res. 129, 1001–1009.

Medlyn, B.E., Badeck, F.W., De Pury, D.G.G., Barton, C.V.M., Broadmeadow, M., Ceulemans, R., De Angelis, P., Forstreuter, M., Jach, M.E., Kellomaki, S., Laitat, E., Marek, M., Philippot, S., Rey, A., Strassemeyer, J., Laitinen, K., Liozon, R., Portier, B., Roberntz, P., Wang, K., Jarvis, P.G., 1999. Effects of elevated $[CO_2]$ on photosynthesis in European forest species: a meta-analysis of model parameters. Plant Cell Environ. 22, 1475–1495.

Medlyn, B.E., Dreyer, E., Ellsworth, D., Forstreuter, M., Harley, P.C., Kirschbaum, M.U. F., Le Roux, X., Montpied, P., Strassemeyer, J., Walcroft, A., Wang, K., Loustau, D., 2002. Temperature response of parameters of a biochemically based model of photosynthesis: II. A review of experimental data. Plant Cell Environ. 25, 1167–1179.

Medlyn, B.E., Duursma, R.A., Eamus, D., Ellsworth, D.S., Prentice, I.C., Barton, C.V.M., Crous, K.Y., de Angelis, P., Freeman, M., Wingate, L., 2011. Reconciling the optimal

and empirical approaches to modelling stomatal conductance. Global Change Biol. 17, 2134–2144.
Misson, L., Tu, K.P., Boniello, R.A., Goldstein, A.H., 2006. Seasonality of photosynthetic parameters in a multi-specific and vertically complex forest ecosystem in the Sierra Nevada of California. Tree Physiol. 26, 729–741.
Mo, X.G., Chen, J.M., Ju, W.M., Black, T.A., 2008. Optimization of ecosystem model parameters through assimilating eddy covariance flux data with an ensemble Kalman filter. Ecol. Modell. 217, 157–173.
Monteith, J.L., 1965. Evaporation and environment. Symp. Soc. Exp. Biol. 19, 205–224.
Ng, G.H.C., Mclaughlin, D., Entekhabi, D., Ahanin, A., 2011. The role of model dynamics in ensemble Kalman filter performance for chaotic systems. Tellus A 63, 958–977.
Norman, J.M., 1982. Simulation of microclimates. In: Jerry, H. (Ed.), Biometeorology in Integrated Pest Management. Academic Press, pp. 65–99.
Pauwels, V.R.N., Verhoest, N.E.C., De Lannoy, G.J.M., Guissard, V., Lucau, C., Defourny, P., 2007. Optimization of a coupled hydrology-crop growth model through the assimilation of observed soil moisture and leaf area index values using an ensemble Kalman filter. Water Resour. Res. 43.
Peichl, M., Arain, M.A., Brodeur, J.J., 2010. Age effects on carbon fluxes in temperate pine forests. Agric. For. Meteorol. 150, 1090–1101.
Pipunic, R.C., Walker, J.P., Western, A., 2008. Assimilation of remotely sensed data for improved latent and sensible heat flux prediction: a comparative synthetic study. Remote Sens. Environ. 112, 1295–1305.
Pregitzer, K.S., King, J.S., Burton, A.J., Shannon, E.B., 2000. Research review: responses of tree fine roots to temperature. New Phytol. 147, 105–115.
Rayner, P.J., 2010. The current state of carbon-cycle data assimilation. Curr. Opin. Environ. Sustainability 2, 289–296.
Reichstein, M., Tenhunen, J., Roupsard, O., Ourcival, J.M., Rambal, S., Miglietta, F., Peressotti, A., Pecchiari, M., Tirone, G., Valentini, R., 2003. Inverse modeling of seasonal drought effects on canopy CO_2/H_2O exchange in three Mediterranean ecosystems. J Geophys. Res. 108.
Sellers, P.J., Randall, D.A., Collatz, G.J., Berry, J.A., Field, C.B., Dazlich, D.A., Zhang, C., Collelo, G.D., Bounoua, L., 1996. A revised land surface parameterization (SiB_2) for atmospheric GCMs . 1. Model formulation. J. Clim. 9, 676–705.
Stoy, P.C., Dietze, M.C., Richardson, A.D., Vargas, R., Barr, A.G., Anderson, R.S., Arain, M.A., Baker, I.T., Black, T.A., Chen, J.M., Cook, R.B., Gough, C.M., Grant, R.F., Hollinger, D.Y., Izaurralde, R.C., Kucharik, C.J., Lafleur, P., Law, B.E., Liu, S., Lokupitiya, E., Luo, Y., Munger, J.W., Peng, C., Poulter, B., Price, D.T., Ricciuto, D. M., Riley, W.J., Sahoo, A.K., Schaefer, K., Schwalm, C.R., Tian, H., Verbeeck, H., Weng, E., 2013. Evaluating the agreement between measurements and models of net ecosystem exchange at different times and timescales using wavelet coherence: an example using data from the North American Carbon Program Site-Level Interim Synthesis. Biogeosciences 10, 6893–6909.
Vicente-Serrano, S.M., Gouveia, C., Camarero, J.J., Begueria, S., Trigo, R., Lopez-Moreno, J.I., Azorin-Molina, C., Pasho, E., Lorenzo-Lacruz, J., Revuelto, J., Moran-Tejeda, E., Sanchez-Lorenzo, A., 2013. Response of vegetation to drought time-scales across global land biomes. Proc. Natl. Acad. Sci. U. S. A. 110, 52–57.
Wang, Y.P., Baldocchi, D., Leuning, R., Falge, E., Vesala, T., 2007. Estimating parameters in a land-surface model by applying nonlinear inversion to eddy covariance flux measurements from eight FLUXNET sites. Global Change Biol. 13, 652–670.
Wang, Y.P., Leuning, R., 1998. A two-leaf model for canopy conductance, photosynthesis and partitioning of available energy I: model description and comparison with a multi-layered model. Agric. For. Meteorol. 91, 89–111.
Wang, Y.P., Leuning, R., Cleugh, H.A., Coppin, P.A., 2001. Parameter estimation in surface exchange models using nonlinear inversion: how many parameters can we estimate and which measurements are most useful? Global Change Biol. 7, 495–510.
Wilson, K.B., Baldocchi, D.D., Hanson, P.J., 2000. Spatial and seasonal variability of photosynthetic parameters and their relationship to leaf nitrogen in a deciduous forest. Tree Physiol. 20, 565–578.
Wolf, A., Akshalov, K., Saliendra, N., Johnson, D.A., Laca, E.A., 2006. Inverse estimation of Vcmax, leaf area index, and the Ball-Berry parameter from carbon and energy fluxes. J. Geophys. Res. 111.
Xu, L.K., Baldocchi, D.D., 2003. Seasonal trends in photosynthetic parameters and stomatal conductance of blue oak (*Quercus douglasii*) under prolonged summer drought and high temperature. Tree Physiol. 23, 865–877.
Yasumura, Y., Hikosaka, K., Hirose, T., 2006. Seasonal changes in photosynthesis, nitrogen content and nitrogen partitioning in Lindera umbellata leaves grown in high or low irradiance. Tree Physiol. 26, 1315–1323.
Zhou, S.X., Duursma, R.A., Medlyn, B.E., Kelly, J.W.G., Prentice, I.C., 2013. How should we model plant responses to drought? An analysis of stomatal and non-stomatal responses to water stress. Agric. For. Meteorol. 182, 204–214.
Zhu, L., Chen, J.M., Qin, Q.M., Li, J.P., Wang, L.X., 2009. Optimization of ecosystem model parameters using spatio-temporal soil moisture information. Ecol. Modell. 220, 2121–2136.